Geophysical Research Letters

RESEARCH LETTER
10.1029/2018GL077609

Key Points:
- We applied fractal geometry to characterize the clustering and rupture radius distribution of observed microseismicity in the Basel EGS
- We generated fractal patterns of fracture networks to simulate the resulting spatial patterns of induced events
- A statistical model is presented to forecast the seismicity based on early stimulation patterns

Supporting Information:
- Supporting Information S1

Correspondence to:
M. J. Afshari Moein,
mohammad.moein@erdw.ethz.ch

Citation:
Afshari Moein, M. J., Tormann, T., Valley, B., & Wiemer, S. (2018). Maximum magnitude forecast in hydraulic stimulation based on clustering and size distribution of early microseismicity. *Geophysical Research Letters*, *45*. https://doi.org/10.1029/2018GL077609

Received 24 FEB 2018
Accepted 29 JUN 2018
Accepted article online 6 JUL 2018

Maximum Magnitude Forecast in Hydraulic Stimulation Based on Clustering and Size Distribution of Early Microseismicity

Mohammad Javad Afshari Moein[1], Thessa Tormann[2], Benoît Valley[3], and Stefan Wiemer[2]

[1]Department of Earth Sciences, Geological Institute, ETH Zürich, Zurich, Switzerland, [2]Department of Earth Sciences, Swiss Seismological Service (SED), ETH Zürich, Zurich, Switzerland, [3]Center for Hydrogeology and Geothermics, University of Neuchâtel, Neuchâtel, Switzerland

Abstract We interpreted the spatial clustering and size distribution of induced microseismicity observed during the stimulation of an enhanced geothermal system beneath Basel by comparison with scale-invariant synthetic data derived from discrete fracture network models. We evaluated microseimic specific influential factors including the effect of hypocentral location uncertainties, existence of a fractured zone and repeating events on the observed spatial organization. Using a dual power-law model originally developed in the context of discrete fracture network modeling, we developed theoretically the relationships among spatial clustering and magnitude distributions. We applied this model to the Basel data set and showed that the spatial clustering characteristics presented stationary properties during the hydraulic stimulation. Based on this observation, we proposed a statistical seismicity model calibrated on the scaling of early stimulation spatial patterns that is capable of forecasting the maximum magnitude of induced events with increasing injection time and stimulated volume.

Plain Language Summary Developing enhanced geothermal systems requires permeability enhancement by hydraulic stimulation, in which pressurized fluid is circulated between injection and production wells. This operation induces microseismicity that may be large enough to be felt by public and result in destructive events. Here we studied the possibility to forecast the maximum magnitude of induced events using the early seismicity patterns during hydraulic stimulation operations. Therefore, we analyzed the spatial clustering and size distribution of induced microseismicity observed during the stimulation of an enhanced geothermal system beneath Basel by comparison with synthetic data derived from fracture network models. We proposed a statistical model, originally developed in the context of discrete fracture network modeling, to represent the clustering and magnitude distribution of induced events. We calibrated the model using the scaling of early stimulation spatial patterns on Basel data set and successfully reproduced the rupture radius distribution, which was also capable of forecasting the maximum magnitude of induced events with increasing injection time and stimulated volume.

1. Introduction

Developing enhanced geothermal systems (EGS) requires massive fluid injections (hydraulic stimulation) to enhance the permeability in order to achieve higher flow rates and exploit the stored heat from elevated temperatures in the Earth's crust. Since the stress conditions of corresponding depths can be critical (Townend & Zoback, 2000), the pressurized fluid injections induce microseismic activity. The associated microseismicity can be large enough to be felt by public and may lead to suspension of geothermal developments such as Saint-Gallen and Basel geothermal projects in Switzerland (Edwards et al., 2015; Häring et al., 2008). The underlying mechanisms of permeability creation during a hydraulic stimulation experiment are not fully understood and still debated. Nevertheless, shearing on rough surfaces due to the increase of pore pressure is expected to enhance the hydraulic conductivity (Evans, Genter, & Sausse, 2005). Induced microseismicity is a result of the interaction between preexisting fracture network and fluid pressure-induced changes (Evans, Moriya, et al., 2005). To reliably assess the rock mass response to fluid injection, the permeability creation potential and the seismic hazard risk of any development scenarios, the 3-D structure of the underlying fracture network should be characterized. Borehole image logs provide the location and orientation of fractures on borehole wall, which are not sufficient to create a 3-D structural model of a reservoir in a depth of 2–5 km (Valley & Evans, 2015). The major unknown parameter of the existing network is fracture length distribution, which has a large impact on the fracture network connectivity and hydraulic

characteristics of rock mass. Induced microseismicity provides valuable information about the possible failure planes within the reservoir volume and this information can be possibly used to guide the stochastic realizations known as discrete fracture networks (DFNs).

Induced microearthquakes reveal scale-invariant spatial patterns (Sahimi et al., 1993; Tafti et al., 2013), and the magnitude frequency relation exhibits power-law distributions (Bachmann et al., 2012; Gutenberg & Richter, 1954). We adopt the working hypothesis that the scaling of induced events is reflecting some aspects of the geometry of underlying fracture network. On the other hand, the fracture networks in geological formations also reveal scale invariant characteristics (Bour & Davy, 1999; Bour et al., 2002; Davy et al., 1990; de Dreuzy et al., 2001, 2002; Lei et al., 2015; Odling et al., 1999). Self-similar fracture patterns may originate from complex self-organized critical dynamics, which relate the large-scale statistics to smaller ones (Allegre et al., 1982; Bak et al., 1988; Sornette, 2006; Sornette et al., 1990). Furthermore, the stress interactions in fractures growth process may also result in power-law length distributions (Davy et al., 2010; Spyropoulos et al., 2002).

The interaction between fluid pressure, in situ stress conditions and fracture network results in microseismicity, which is not completely understood. Potential similarities between the scaling properties of fracture networks and induced microseismicity may improve the statistical seismicity models. Current statistical models typically neglect the scaling properties of microseismic patterns and potential correlations between location and magnitude of induced events. Moreover, these statistical models are mostly unable to explain the effect of geological features such as damage zones and geophysical features such as location uncertainties and repeating events on the scaling properties of induced patterns. Proper understanding of the scaling characteristics of microseismicity patterns may introduce new features into the statistical models and improve the maximum magnitude forecast during hydraulic stimulation operations.

We implement fractal geometry to characterize the spatial distribution of microseismicity in the Basel geothermal site and analyze the scaling properties by simulating the previously mentioned microseismic specific features. Such analyses lead to propose a statistical model that presents the spatial clustering and rupture size distribution of induced events. The parameters of this model are calibrated by early time patterns (learning phase) and forecast the seismic risk during the continued injection and shut-in phase. We test this model in the Basel geothermal site and conclude with an outlook for future applications.

2. Microseismicity in Basel Geothermal Site

Injecting water at high pressure into the open hole section below 4,629 m of Basel geothermal system induced 14,578 recorded seismic events between 2 December 2006 and 31 March 2007; 3,460 of which were located (Dyer et al., 2010; Häring et al., 2008). Kraft and Deichmann (2014) performed a waveform similarity analysis and relocated the initial catalogue to 1980 events and reduced the uncertainty of hypocentral locations. We use this catalogue in this study. Figure 1a displays the spatial scattering of microearthquake hypocenters from top and side view, and Figure 1b shows the corresponding cumulative frequency size distribution with the estimate of b value using the maximum likelihood fit (Aki, 1965).

2.1. Spatial Distribution

Two-point correlation function has been widely used to characterize the spatial clustering of fractures and earthquake hypocenters (Bour et al., 2002; Hirata et al., 1987). Among different techniques reported in literature, this function delivers the most reliable and stationary exponents of spatial distributions and is less affected by finite size effects. Bour et al. (2002) has verified this statement on characterizing the spatial distribution of fractures in Hornelen Basin. A fractal dimension (D_2) is computed by fitting a power law to correlation function according to equation (1),

$$C(r) = \frac{2}{N(N-1)} N_p(r) \sim r^{D_2} \tag{1}$$

where N is the total number of events and N_p is the number of pairs of events whose hypocentral distance is less than r (Hentschel & Procaccia, 1983). Figure 1c represents the correlation function of induced events in the Basel EGS site. The corresponding local slope is close to two between 50 and 100 m distance then decreases between 2 and 50 m and larger than 100 m. Therefore, such a deviation from pure scaling law should be explained.

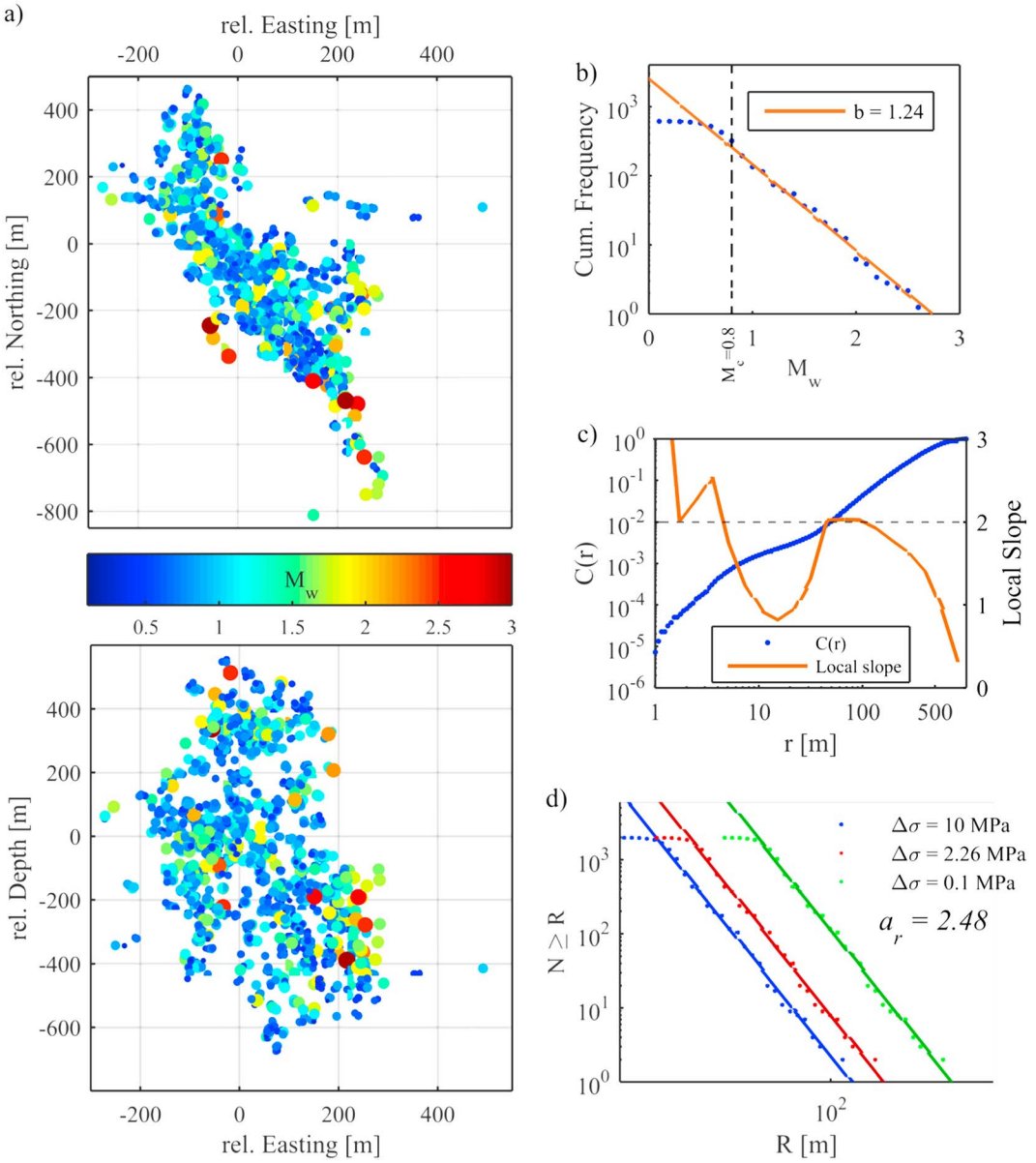

Figure 1. (a) Top and side views of the spatial scattering of microearthquake hypocenters relative to the casing shoe in Basel geothermal system (Kraft & Deichmann, 2014). (b) Frequency-size distribution of microearthquakes and estimates of b value using maximum likelihood estimates. (c) Correlation function and its local slope. (d) Complementary cumulative rupture radius distribution (R) for different stress drops.

2.2. Rupture Radius Distribution

Most seismic events in hydraulic stimulation represent failures on existing fracture planes and the reported magnitude depends on the radius of the rupture plane and the stress drop. If we assume every event represents a rupture plane, a rupture radius can be assigned by equation (2). The radius of a circular failure plane (R) in space is related to stress drop ($\Delta\sigma$) and seismic moment (M_0) through equation (2) (Eshelby, 1957),

$$R^3 = \frac{7M_0}{16\Delta\sigma} \tag{2}$$

Goertz-Allmann et al. (2011) determined the stress drops from P wave signals of 1,000 microearthquakes in Basel and a large portion of the events showed a constant stress drop of 2.26 MPa (the average value)

with a variation between 0.1 and 10 MPa. If we simply assume a constant stress drop on every seismic event, the rupture radius scaling exponent a_r may be computed. Figure 1d shows the rupture size distribution of induced events for three different stress drop assumptions (0.1, 2.26, and 10 *MPa*) follows a power law, whose slope a_r is independent from the average stress drop on each event and is related to b value through equation (3) (Shapiro et al., 2013).

$$a_r = 2b + 1 \tag{3}$$

3. Synthetic Fracture Network Model

The evidence on clustering and power-law size distribution of rupture patterns motivates generating synthetic rupture patterns with the same statistical characteristics. Thus, we utilized the concepts developed in the framework of discrete fracture network modeling and adopted the following statistical model to generate fractal fracture patterns from Davy et al. (1990),

$$n(l, L)dl = \alpha L^{D} l^{-a_f} dl \tag{4}$$

where, $n(l, L)dl$ is the number of fractures whose length is in the range $[l, l + dl]$ and whose center belongs to a volume in three dimensions of size L^3 $[m]^3$, α $[m]^{a-D-1}$ is a normalization constant and affects the fracture density, D is the correlation dimension of fracture centers, and a_f is the fracture length exponent. This model, also known as dual-power law model, has been widely used to study different aspects of fractured media (Darcel et al., 2003; Harthong et al., 2012; Kim, 2007; Verscheure et al., 2012). Here the size of a fracture plane is defined as the radius of a circular disk. The motivation to choose such a fracture model is that natural fractures exhibit self-similar spatial patterns in different scales (Chiles, 1988; Davy, 1993). In addition, power-law distribution is the only scale-invariant statistical distribution and has been used to describe the fracture attributes in different scales. Different fracture attributes such as trace length, spacing, RQD (rock quality designation, Deere & Deere, 1988), aperture, and surface roughness show also self-similar patterns (Barton & Zoback, 1992; Boadu & Long, 1994; Bonnet et al., 2001; Power & Tullis, 1991). Dual power-law model enables to generate fractal spatial organization as well as power-law length distribution of fractures in two and three dimensions. We developed this model to generate random network realizations in MATLAB and verified the power-law spatial and size distribution of fractal DFNs, which is presented in the supporting information. In addition, the relation between position and size distribution of fractures is verified in synthetic fracture networks. The details of the generation methodology are available in the above-mentioned references.

The fractal analysis of microseismicity patterns do not present a clear scaling (Figure 1c) and requires further analysis. Here we analyze the influence of three factors that complicate the extraction of geometrical characteristics of fracture network from seismicity data. The factors that we include in this analysis are as follows: (1) uncertainty associated with location of microearthquake hypocenters, (2) existence of a fractured zone, and (3) repeating events on same structures. For this analysis, we generated a 3-D DFN with the following input parameters $D = 2.7$, $a = 3.5$, $\alpha = 0.1$, $l_{min} = 10$ m in a cubic domain with side length of $L = 500$ m. We need to mention that no boundary treatment is done, that is, some fractures might extend outside of the generation domain.

3.1. Uncertainty of Hypocentral Locations

Earthquake locations are estimated by travel time inversion of the recorded *P* wave and *S* wave arrivals. The computed hypocenters are associated with uncertainties because of unknown velocity structure of the earth and arrival time observation errors. The confidence region of earthquake hypocenters are ellipsoidal and normally distributed (Husen & Hardebeck, 2010). The variance of the normally distributed earthquake hypocenters can be determined by a principal component analysis of the scatter clouds obtained from random realizations of hypocenters locations considering uncertainties on the seismic data and velocity model. The 68% confidence level of principal axes of ellipsoids in Basel geothermal system have a mean length of 74, 48, and 32 m which, are taken from a principal component analysis of the scatter clouds (Kraft & Deichmann, 2014).

To study the influence of such an uncertainty, we insert a random noise on fracture center coordinates (XYZ) from a normal distribution in the 3-D fracture network of Figure 2a. If the principal axes of ellipsoids are

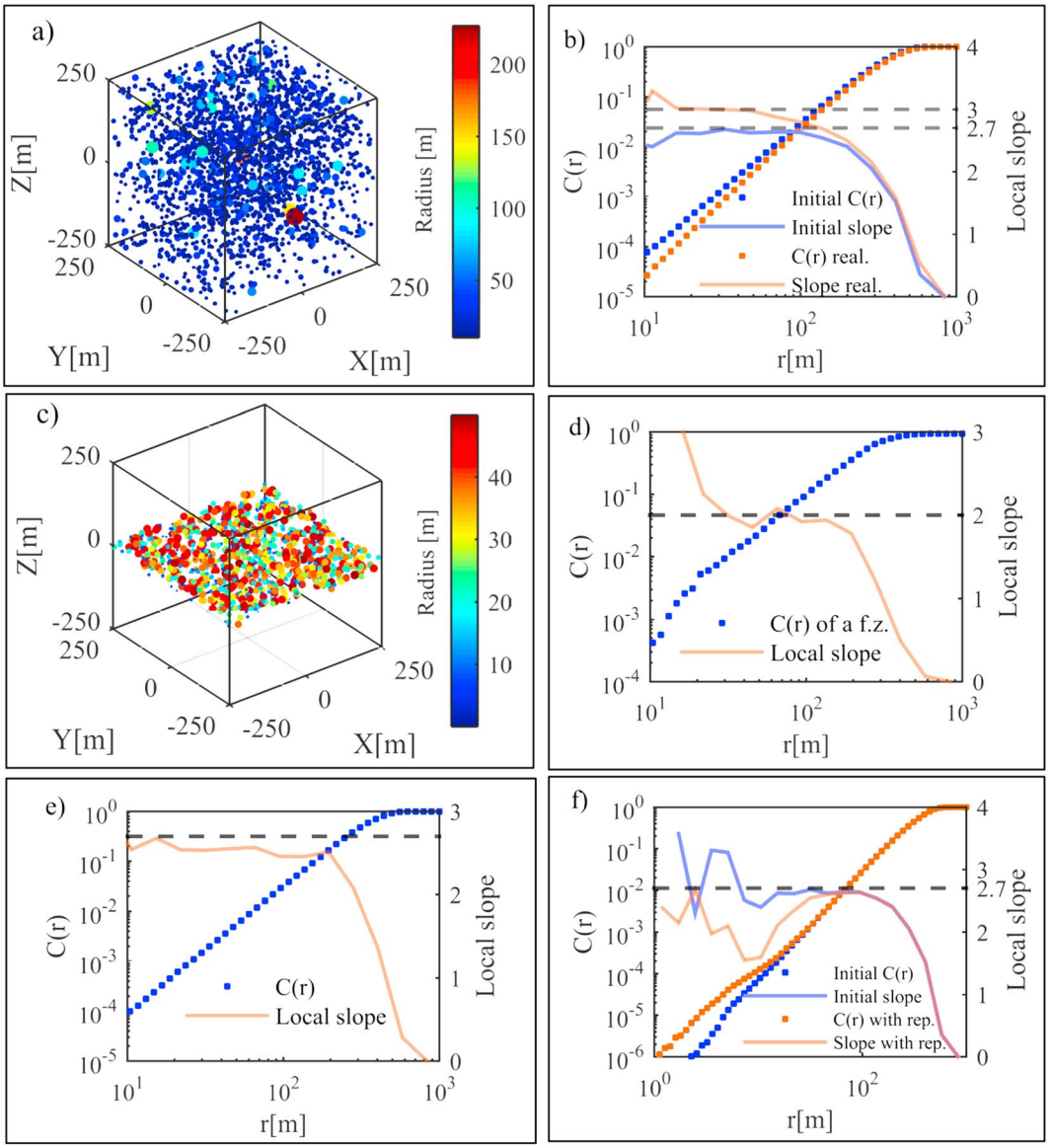

Figure 2. (a) A 3-D random DFN with $D = 2.7$, $a = 3.5$, and $\alpha = 0.1$. (b) Effect of 93 m uncertainty in fracture center locations on the resulting spatial distribution of a random realization of the initial network. (c) 3-D view of a 40-m-width fractured zone. (d) Spatial organization of a fractured zone. (e) Spatial organization of the network merging two networks in (a) and (c). (f) Effect of 100 f repeaters in a maximum *5* m distance from 10 randomly selected fractures (10 repeaters belong to each fracture).

aligned with XYZ coordinates, the variance of the noise are 74, 48, and 32 m in the direction of each coordinate (the maximum uncertainty in 3-D is 93 m). Figure 2b shows the correlation function and its local slope of a random realization with predefined noise on fracture center locations compared to initial network. The correlation dimension tends to increase (approach to 3), if the hypocentral location uncertainty is included in the rupture models. A sensitivity analysis on the effect of uncertainty in 3-D is presented in the supporting information.

3.2. Existence of a Fractured Zone

Borehole observations and induced microseismicity in deep crystalline rocks confirm the existence of fractured zones, which provide the main fluid path into the reservoir (Deichmann et al., 2014; Evans, Genter, & Sausse, 2005). Fractured zones are intervals of very high density fractures, where the spatial distribution of fractures can be assumed to be random in a limited width. From the geological perspective, fractured

zones are equivalent to damage zones flanking a fault core with a very high permeability and introducing a preferential fluid flow path (Bense et al., 2013). To simulate a fractured zone, we generate a simple synthetic horizontal fractured zone by populating uniformly distributed fracture centers with a uniform radius between 0 and 50 m in a slice of 40 m width (Figure 2c). Since the focus is on the spatial distribution of fracture centers, the radius distribution does not change the analysis. A fractured zone with 1,000 fracture centers is generated in the domain similar to network of Figure 2a and the corresponding correlation function of the 3-D spatial distribution is displayed in Figure 2d. The correlation dimension of such a fractured zone equals 2.

The fractured zones may be embedded in a 3-D network. Therefore, if we add a fractured zone into the network of Figure 2a, the spatial distribution of the network may be altered. Figure 2e shows the correlation function of the resulting network and its local slope, which is slightly less than 2.7. A sensitivity analysis on the width of fractured zone and its influence on the resulting spatial organization is presented in the supporting information.

3.3. Repeating Events

The source of every recorded microseismic event might not be unique and the rupture might occur on different points of a discontinuity plane. Repeating events are characterized by almost identical waveforms, which reflect very similar re-ruptures of the same structure but may have different magnitudes. Here we analyze the influence of repeating events on the spatial organization of a synthetic fracture network. Therefore, we add random fracture centers representing the repeating events to the network of Figure 2a. We choose 10 random fractures from the initial network and add 10 fracture centers very close to them (entirely 100 random fracture centers represent the repeaters). The repeaters are selected randomly from a sphere with a radius of 4.3 m, perturbed the randomly chosen fractures (i.e., the maximum offset of repeater coordinates from the chosen fracture center is 2.5 m). The correlation function of the initial network with repeaters is displayed in Figure 2f and a sensitivity analysis on the number of repeating events is presented in the supporting information. Introducing the repeaters into the rupture model results in a drop of the correlation dimension in distances between 2 and 100 m.

Here we analyzed the impact of three main factors that may substantially deviate the scaling of microearthquake patterns from a pure power-law. However, other factors may influence the scaling properties of induced patterns. For instance, the orientation of discontinuities relative to the in situ stress conditions may affect the spatial organization of slipping patches. Analyzing the impact of this factor requires physical modeling of the induced seismicity using thermo-hydromechanical simulations, which is beyond the scope of this paper.

4. Geometrical Forecast Approach

In previous sections, we applied synthetic fracture networks to explain the spatial organization of induced events in Basel and described the impact of influential factors. In general, extracting the statistical properties of network geometry from induced microseismicity is difficult, because of the previously discussed factors. Nevertheless, similarities between the induced microseismicity and scale invariant fractal networks motivated us to propose a statistical model for geometry of rupture patterns. This model represents the clustering and size distribution of induced seismicity by a dual power-law model, which is initially developed for fracture networks. This forecast approach is different from other statistical approaches such as the seismicity models presented by Shapiro et al. (2013) and McGarr (2014). The major progress in this model stems from the physical nature that originates from the scaling characteristics of fracture networks. These characteristics enable the model to clarify the effect of features that deviate the microseismicity patterns from pure scaling laws such as repeating events, hypocentral uncertainty, and fractured zones. In a specific comparison to the model proposed by Shapiro et al. (2013), which deals with planar preferential path for the seismicity cloud, dual-power law is a universal model that can include any fractal dimensions between 2 and 3 (2 is a planar structure and 3 is uniformly distributed in space). For instance, the Geyser field (Tafti et al., 2013), in which the spatial distribution of induced events shows a fractal dimension of 2.57.

4.1. Methodology

This approach sets a dual-power law model for rupture patterns based on very early stimulation phase (learning period) and performs a predictive real-time seismic hazard analysis, so that future development of microseismicity can be anticipated. It computes the maximum rupture radius and the corresponding

seismic magnitude (assuming a constant and conservative stress drop) with an increase in the perturbed reservoir volume. We define the *perturbed reservoir volume* as the smallest cubic volume which encompasses all the microearthquake hypocenters. This methodology is based on scale-invariant spatial distribution of seismic events and the power-law rupture radius distribution. In general, a simple dual power-law model can represent the rupture geometry patterns similar to equation (5);

$$n(R,L)dl = \alpha L^{D_r} R^{-a_r} dl \tag{5}$$

where the seismic patterns are located in a cube of side length L with a correlation dimension of D_r and rupture size exponent of a_r. The initial parameters (a_r, D_r, α, and L) of this equation are estimated from the learning phase patterns. We take the maximum offset of seismic events from the casing shoe plus the corresponding location uncertainty as the initial side length of the perturbed volume (L) and set the approximate minimum rupture radius (R_{min}) in the perturbed volume of the learning phase. Magnitude of completeness (M_c) delivers R_{min} using equation (2). For a detailed analysis on how to compute the magnitude of completeness (M_c), we refer to Mignan and Woessner (2012). Finally, the parameter α may be estimated from equation (6).

$$N = \int_{R_{min}}^{\infty} n(R,L)dl = \frac{\alpha}{a_r - 1} L^{D_r} R_{min}^{-(a_r-1)} \tag{6}$$

If the injection continues to sweep a larger volume and increase the perturbed volume with a side length of $L'(L' > L)$, this model can compute the rupture radius distribution and the corresponding size magnitude by equation (7).

$$n(R,L)dl = \alpha (L')^{D_r} R^{-a_r} dl \tag{7}$$

The estimated rupture radius exponent (a_r) is independent from the average stress drop on rupture planes, whereas the minimum and maximum rupture radius depends on the assumed stress drop (Figure 1d). The maximum expected (M_w) should be computed based on the most conservative case, where the stress drop is the largest (e.g., 10 MPa).

4.2. Time Dependency of Clustering and Size Distribution of Seismicity in Basel

Before the application of this methodology to Basel data, we need to study the dependence of clustering and rupture radius distribution on the number of events (increasing time windows). The exponents of D_r and a_r are computed by a linear fit through the linear section of the resulting $C(r)$ and N, starting from the estimated minimum radius. Figure 3a shows that a_r exhibits very little variation during the injection phase and slightly decreases in the post-injection phase (a_r varies between 3.7 and 4.1 in whole seismic activity). This implies that the statistics of larger events (that mostly happen in later stages) may differ from smaller events (early stages). A sensitivity analysis is required to evaluate the applicability of early events to estimate the maximum magnitude as function of perturbed volume. In addition, D_r is very close to 2 with no clear deviations, reflecting a fractured zone (Figure 3b).

4.3. Application to Basel

If we choose the first 100 events as the learning phase and compute the completeness magnitude of $M_c = 0.8$, the corresponding minimum rupture radius for $\Delta\sigma = 10$ MPa equals $R_{min} = 9.5m$. If the events less than M_c are excluded, remaining events are encompassed by a cube, centred in the casing shoe with a side length of $L = 500$ m. To ensure all the ruptures do not extend outside of the seismic volume, we compute $\frac{L}{2}$ by adding the maximum rupture radius and maximum location uncertainty to the maximum distance from the casing shoe. If the average stress drop on every event is 10 MPa, the rupture radius exponent is equal to $a_r = 3.9$. If all the parameters of the rupture model is inserted in equation (5), the resulting α is 0.47 and the seismicity model corresponds to equation (8).

$$n(R,L)dl = 0.47\, L^2 R^{-3.9} dl \tag{8}$$

Figure 3c represents the calibration of rupture model to the learning phase (blue line). If the injection continues to sweep a larger reservoir volume, the rupture size distribution continues to move upwards

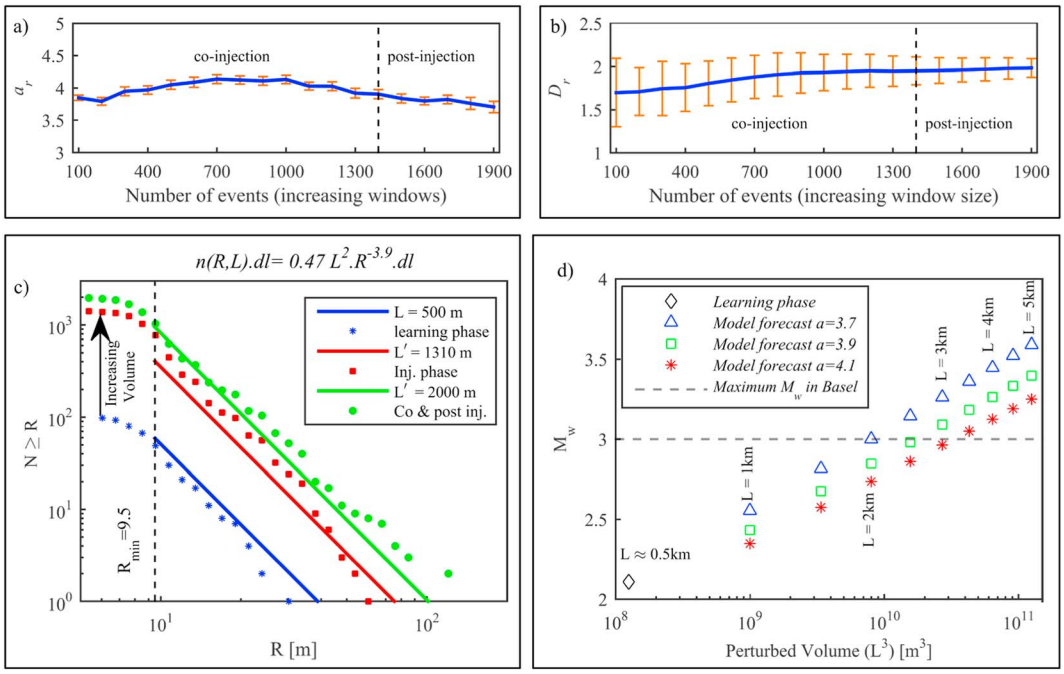

Figure 3. (a) Dependence of rupture radius exponent on the number of events in Basel geothermal site. (b) Dependence of rupture clustering on the number events in Basel. (c) Calibration of the seismicity model to the first 100 events (learning phase) during the injection phase and simulation of rupture radius distribution with increasing the perturbed volume in Basel geothermal reservoir. (d) Prediction of maximum moment magnitude M_w of Basel geothermal reservoir as a function of perturbed volume with an assumption of $\Delta\sigma$ = 10 MPa.

(Figure 3c). During the injection phase, the perturbed volume is a cube of side length L' = 1310 m. If the new L' is replaced in the model, the resulting rupture radius distribution corresponds to Figure 3c (red line). Although the injection has stopped in this step, the fluid is still sweeping a larger reservoir volume, which is verified by the corresponding microseismicity patterns which are growing, and the corresponding perturbed volume of L' = 2,000 m (green line).

For a seismic hazard assessment, the maximum expected magnitude can be estimated based on a conservative stress drop of 10 MPa. Figure 3d represents maximum M_w as a function of perturbed volume for three different rupture exponents of 3.7, 3.9, and 4.1. The sensitivity analysis shows that the maximum magnitude forecast based on the learning phase (green squares) is not significantly different from to magnitude corresponding to the exponent of 3.7 (blue triangles) for a perturbed volume of approximately 10^{10} m^3. We choose a random realization in which the large events do not extend outside of the seismic volume. However, this does not affect the maximum magnitude forecast.

5. Discussion and Conclusion

Two-point correlation function of microearthquake hypocenters in the Basel EGS reservoir showed a complicated behavior, which is not completely linear in a logarithmic scale. Furthermore, the estimated rupture radius of every seismic event follows a power law, whose slope is independent from the average stress drop on each event. When assuming a constant stress drop on all fracture planes, the resulting ruptures most probably exhibit the statistics of the fracture network. One explanation may be the power-law fracture nature of length distribution in geological formations. Although the scaling exponent does not vary with a change in the average stress drop, but the power-law range varies (particularly the minimum rupture radius). Higher stress drops correspond to smaller rupture sizes and vice versa. These observations supported the hypothesis that scaling properties of fracture networks are similar to the scaling of microseismicity patterns.

To interpret the clustering and size distribution of induced events, we generated synthetic fracture networks as a representative of rupture planes. We simulated the factors that complicate the potential relations between the induced microseismicity and fracture network. Hypocentral locations are quantified by a principal component analysis of the scatter clouds. If the uncertainty of the earthquake hypocenter is included in a synthetic fractal DFN by imposing the statistical distribution of error estimates (normal distributed inside the uncertainty ellipsoids), the resulting correlation dimension increases and approaches to a randomly distributed pattern ($D = 3$). However, the increase of randomness depends on the variance of hypocentral coordinates in each direction. In addition, a hydraulic stimulation in a fractured zone might change the 3-D spatial distribution from the ideal pattern fracture network pattern. In this case, the correlation dimension of the microearthquakes is very close to 2 (similar to the relocated microseismicity patterns in Basel). Furthermore, adding a fractured zone into a 3-D fractal pattern, results in decreasing the correlation dimensions. The third factor in our study was repeating events, which change the spatial distribution and create a sudden drop in the computed correlation dimension. Since the magnitude of repeating events are not necessarily the same, the effect of repeating events on the rupture radius distribution is not clear. To summarize, hypocentral uncertainty, presence of a fractured zone and repeating events complicate the interpretation of spatial patterns of induced seismicity and the correspondence to the underlying fracture network.

Synthetic networks reveal the restrictions associated with extracting the fracture network geometry from microseismic data. Despite these complexities, the scaling properties of induced seismicity and synthetic fracture networks are very similar. A dual power-law model representing the rupture clustering and size distribution can be applied for modeling the induced microseismicity. This model adds physical representation to the rupture planes as pre-existing fractures, explains the effect of geological and geophysical factors on the scaling properties of induced patterns. Finally, it introduces a universal model that is capable to model clusters with fractal dimension between 2 and 3.

The model parameters must be calibrated on the scaling properties of learning phase. We applied this model to forecast the induced seismicity in Basel geothermal reservoir to assess the seismic hazard of hydraulic stimulation. A reanalysis of Basel microseismicity patterns confirms the independence of clustering from the cumulative number of events. Thus, early stimulation events can exhibit the scaling characteristics of rupture patterns in perturbed reservoir volume. In this case, a learning phase of early first 100 events were applied to set up the model. The seismic hazard assessment is based on the highest reported stress drop in Basel ($\Delta\sigma = 10$ MPa). If the injection continues to sweep a larger volume, the seismicity model could forecast the highest rupture radius from the associated rupture size distribution and estimate the corresponding seismic magnitude (M_w). This model could predict the statistics of seismicity during the co-injection phase as a function of the perturbed volume. The post-injection phase shows slightly different statistics, which may be due to the different stress conditions prevailing in the co-injection and post-injection phases (shut-in and bleed-off phase). Despite the differences, this model was able to reproduce a similar rupture distribution for the co-injection and post-injection phases. Ultimately, the maximum expected magnitude showed a power-law relation with the perturbed reservoir volume in the Basel site. A sensitivity analysis on the rupture exponents revealed the maximum magnitude estimation is not significantly different from the upper bound, which confirms the applicability of this approach for the typical hydraulic stimulations. This difference increases if the perturbed volume is increasing. However, the real-time update of rupture exponent during the hydraulic stimulations and expansion of the learning phase would improve the forecasts.

Acknowledgments

We would like to thank Simon Löw and Keith Evans for scientific support during this research. Furthermore, we are grateful to Philippe Davy and Caroline Darcel for constructive and critical comments. The research leading to these results has received funding from the European Community's Seventh Framework Program under grant agreement 608553 (Project IMAGE). Furthermore, we would like to confirm that the readers can access any data provided in the paper.

References

Aki, K. (1965). Maximum likelihood estimate of b in the formula log N = a-bM and its confidence limits. *Bulletin of the Earthquake Research Institute, Tokyo University*, *43*, 237–239.

Allegre, C. J., Lemouel, J. L., & Provost, A. (1982). Scaling rules in rock fracture and possible implications for earthquake prediction. *Nature*, *297*(5861), 47–49. https://doi.org/10.1038/297047a0

Bachmann, C. E., Wiemer, S., Goertz-Allmann, B., & Woessner, J. (2012). Influence of pore-pressure on the event-size distribution of induced earthquakes. *Geophysical Research Letters*, *39*, L09302. https://doi.org/10.1029/2012GL051480

Bak, P., Tang, C., & Wiesenfeld, K. (1988). Self-organized criticality. *Physical Review A*, *38*(1), 364–374. https://doi.org/10.1103/PhysRevA.38.364

Barton, C. A., & Zoback, M. D. (1992). Self-similar distribution and properties of macroscopic fractures at depth in crystalline rock in the Cajon Pass scientific drill hole. *Journal of Geophysical Research*, *97*, 5181–5200. https://doi.org/10.1029/91JB01674

Bense, V., Gleeson, T., Loveless, S., Bour, O., & Scibek, J. (2013). Fault zone hydrogeology. *Earth-Science Reviews*, *127*, 171–192. https://doi.org/10.1016/j.earscirev.2013.09.008

Boadu, F., & L. Long (1994). The fractal character of fracture spacing and RQD, paper presented at International journal of rock mechanics and mining sciences & geomechanics abstracts, Elsevier.

Bonnet, E., Bour, O., Odling, N. E., Davy, P., Main, I., Cowie, P., & Berkowitz, B. (2001). Scaling of fracture systems in geological media. *Reviews of Geophysics*, *39*, 347–383. https://doi.org/10.1029/1999RG000074

Bour, O., & Davy, P. (1999). Clustering and size distributions of fault patterns: Theory and measurements. *Geophysical Research Letters*, *26*, 2001–2004. https://doi.org/10.1029/1999GL900419

Bour, O., Davy, P., Darcel, C., & Odling, N. (2002). A statistical scaling model for fracture network geometry, with validation on a multiscale mapping of a joint network (Hornelen Basin, Norway). *Journal of Geophysical Research*, *107*(B6), 2113. https://doi.org/10.1029/2001JB000176

Chiles, J. (1988). Fractal and geostatistical methods for modeling of a fracture network. *Mathematical Geology*, *20*(6), 631–654. https://doi.org/10.1007/BF00890581

Darcel, O. B., Davy, P., & de Dreuzy, J. R. (2003). Connectivity properties of two-dimensional fracture networks with stochastic fractal correlation. *Water Resources Research*, *39*(10), 1272. https://doi.org/10.1029/2002WR001628

Davy, P., Sornette, A., & Sornette, D. (1990). Some consequences of a proposed fractal nature of continental faulting. *Nature*, *348*(6296), 56–58. https://doi.org/10.1038/348056a0

Davy, P. (1993). On the frequency-length distribution of the San Andreas fault system. *Journal of Geophysical Research*, *98*, 12,141–12,151. https://doi.org/10.1029/93JB00372

Davy, R. L. G., Darcel, C., Bour, O., De Dreuzy, J.-R., & Munier, R. (2010). A likely universal model of fracture scaling and its consequence for crustal hydromechanics. *Journal of Geophysical Research*, *115*, B10411. https://doi.org/10.1029/2009JB007043

de Dreuzy, J. R., Davy, P., & Bour, O. (2002). Hydraulic properties of two-dimensional random fracture networks following power law distributions of length and aperture. *Water Resources Research*, *38*(12), 1276. https://doi.org/10.1029/2001WR001009

de Dreuzy, J.-R., Davy, P., & Bour, O. (2001). Hydraulic properties of two-dimensional random fracture networks following a power law length distribution 1. Effective connectivity. *Water Resources Research*, *37*, 2065–2078. https://doi.org/10.1029/2001WR900011

Deere, D., & D. Deere (1988). The rock quality designation (RQD) index in practice, paper presented at Symposium on Rock Classification Systems for Engineering Purposes, 1987, Cincinnati, Ohio, USA.

Deichmann, N., Kraft, T., & Evans, K. F. (2014). Identification of faults activated during the stimulation of the Basel geothermal project from cluster analysis and focal mechanisms of the larger magnitude events. *Geothermics*, *52*, 84–97. https://doi.org/10.1016/j.geothermics.2014.04.001

Dyer, B. C., Schanz, U., Spillmann, T., Ladner, F., & Häring, M. O. (2010). Application of microseismic multiplet analysis to the Basel geothermal reservoir stimulation events. *Geophysical Prospecting*, *58*(5), 791–807. https://doi.org/10.1111/j.1365-2478.2010.00902.x

Edwards, B., Kraft, T., Cauzzi, C., Kästli, P., & Wiemer, S. (2015). Seismic monitoring and analysis of deep geothermal projects in St Gallen and Basel, Switzerland. *Geophysical Journal International*, *201*(2), 1022–1039. https://doi.org/10.1093/gji/ggv059

Eshelby, J. D. (1957). The determination of the elastic field of an ellipsoidal inclusion, and related problems, paper presented at Proceedings of the Royal Society of London A: Mathematical, Physical and Engineering Sciences, The Royal Society.

Evans, H., Moriya, H., Niitsuma, R. H., Jones, W. S., Phillips, A., Genter, J., et al. (2005). Microseismicity and permeability enhancement of hydrogeologic structures during massive fluid injections into granite at 3 km depth at the Soultz HDR site. *Geophysical Journal International*, *160*(1), 389–412. https://doi.org/10.1111/j.1365-246X.2004.02474.x

Evans, K. F., Genter, A., & Sausse, J. (2005). Permeability creation and damage due to massive fluid injections into granite at 3.5 km at Soultz: 1. Borehole observations. *Journal of Geophysical Research*, *110*, B04204. https://doi.org/10.1029/2004JB003168

Goertz-Allmann, B. P., Goertz, A., & Wiemer, S. (2011). Stress drop variations of induced earthquakes at the Basel geothermal site. *Geophysical Research Letters*, *38*, L09308. https://doi.org/10.1029/2011GL047498

Gutenberg, B., & Richter, C. (1954). *Seismicity of the Earth and associated phenomena*. New York: Princeton University Press.

Häring, M. O., Schanz, U., Ladner, F., & Dyer, B. C. (2008). Characterisation of the Basel 1 enhanced geothermal system. *Geothermics*, *37*(5), 469–495. https://doi.org/10.1016/j.geothermics.2008.06.002

Harthong, B., Scholtès, L., & Donzé, F.-V. (2012). Strength characterization of rock masses, using a coupled DEM–DFN model. *Geophysical Journal International*, *191*(2), 467–480. https://doi.org/10.1111/j.1365-246X.2012.05642.x

Hentschel, H. G. E., & Procaccia, I. (1983). The infinite number of generalized dimensions of fractals and strange attractors. *Physica D: Nonlinear Phenomena*, *8*(3), 435–444. https://doi.org/10.1016/0167-2789(83)90235-X

Hirata, T., Satoh, T., & Ito, K. (1987). Fractal structure of spatial distribution of microfracturing in rock. *Geophysical Journal International*, *90*(2), 369–374. https://doi.org/10.1111/j.1365-246X.1987.tb00732.x

Husen, S., & Hardebeck, J. (2010). Earthquake location accuracy, Community Online Resource for Statistical Seismicity Analysis. https://doi.org/10.5078/corssa-55815573. Retrieved from http://www.corssa.org

Kim, T. H. (2007). *Fracture characterization and estimation of fracture porosity of naturally fractured reservoirs with no matrix porosity using stochastic fractal models*. Texas A&M Univ.

Kraft, T., & Deichmann, N. (2014). High-precision relocation and focal mechanism of the injection-induced seismicity at the Basel EGS. *Geothermics*, *52*, 59–73. https://doi.org/10.1016/j.geothermics.2014.05.014

Lei, Q., Latham, J. P., Tsang, C. F., Xiang, J., & Lang, P. (2015). A new approach to upscaling fracture network models while preserving geostatistical and geomechanical characteristics. *Journal of Geophysical Research: Solid Earth*, *120*, 4784–4807. https://doi.org/10.1002/2014JB011736

McGarr, A. (2014). Maximum magnitude earthquakes induced by fluid injection. *Journal of Geophysical Research: Solid Earth*, *119*, 1008–1019. https://doi.org/10.1002/2013JB010597

Mignan, A., & Woessner, J. (2012). Estimating the magnitude of completeness for earthquake catalogs. *Community Online Resource for Statistical Seismicity Analysis*, https://doi.org/10.5078/corssa-00180805. Retrieved from http://www.corssa.org

Odling, P., Gillespie, B., Bourgine, C., Castaing, J., Chiles, N., Christensen, E., et al. (1999). Variations in fracture system geometry and their implications for fluid flow in fractured hydrocarbon reservoirs. *Petroleum Geoscience*, *5*(4), 373–384. https://doi.org/10.1144/petgeo.5.4.373

Power, W. L., & Tullis, T. E. (1991). Euclidean and fractal models for the description of rock surface roughness. *Journal of Geophysical Research*, *96*, 415–424. https://doi.org/10.1029/90JB02107

Sahimi, M., Robertson, M. C., & Sammis, C. G. (1993). Fractal distribution of earthquake hypocenters and its relation to fault patterns and percolation. *Physical Review Letters*, *70*(14), 2186–2189. https://doi.org/10.1103/PhysRevLett.70.2186

Shapiro, S. A., Krüger, O. S., & Dinske, C. (2013). Probability of inducing given-magnitude earthquakes by perturbing finite volumes of rocks. *Journal of Geophysical Research: Solid Earth*, *118*, 3557–3575. https://doi.org/10.1002/jgrb.50264

Sornette, D. (2006). *Critical phenomena in natural sciences: chaos, fractals, self organization and disorder: Concepts and tools*. New York: Springer Science & Business Media.

Sornette, D., Davy, P., & Sornette, A. (1990). Structuration of the lithosphere in plate tectonics as a self-organized critical phenomenon. *Journal of Geophysical Research: Solid Earth*, *95*, 17,353–17,361. https://doi.org/10.1029/JB095iB11p17353

Spyropoulos, C., Scholz, C. H., & Shaw, B. E. (2002). Transition regimes for growing crack populations. *Physical Review E*, *65*(5), 056105. https://doi.org/10.1103/PhysRevE.65.056105

Tafti, T. A., Sahimi, M., Aminzadeh, F., & Sammis, C. G. (2013). Use of microseismicity for determining the structure of the fracture network of large-scale porous media. *Physical Review E*, *87*(3), 032152. https://doi.org/10.1103/PhysRevE.87.032152

Townend, J., & Zoback, M. D. (2000). How faulting keeps the crust strong. *Geology*, *28*(5), 399–402. https://doi.org/10.1130/0091-7613(2000)28<399:HFKTCS>2.0.CO;2

Valley, B., & Evans, K. (2015). Methods for characterizing deep geothermal reservoirs from borehole measurements. In S. Hirschberg, S. Wiemer, & P. Burgherr (Eds.), *Energy from the Earth* (pp. 64–81). Zürich: vdf Hochschulverlag.

Verscheure, M., Fourno, A., & Chilès, J.-P. (2012). Joint inversion of fracture model properties for CO_2 storage monitoring or oil recovery history matching. *Oil & Gas Science and Technology–Revue d'IFP Energies nouvelles*, *67*(2), 221–235. https://doi.org/10.2516/ogst/2011176